Effects of intratidal and tidal range variability on circulation and salinity structure in the Cape Fear River Estuary, North Carolina

May Ling Becker,[1] Richard A. Luettich Jr.,[2] and Harvey Seim[1]

Received 17 June 2008; revised 5 November 2008; accepted 27 January 2009; published 21 April 2009.

[1] Tidal influences on circulation and the salinity structure are investigated in the largely unstudied Cape Fear River Estuary (CFRE), North Carolina, a partially mixed estuary along the southeast coast of the United States. During two different tidal conditions (high versus low tidal range) and when river flow was low, salinity and velocity data were collected over a semidiurnal tidal cycle in a 2.8 km long transect along the estuary axis. Water level data were recorded nearby. Mechanisms that influence salt transport characteristics are diagnosed from an analysis of the field data. Specifically, we investigated the relationship between tidal range and salinity through comparison of along-channel circulation characteristics, computed salt fluxes, and coefficients of vertical eddy diffusivity (K_z) based on a parameterization and on salt budget analysis. Findings indicate up-estuary tidally driven salt fluxes resulting from oscillatory salt transport are dominant near the pycnocline, while mean advective transport dominates near the bottom during both tidal range periods. Earlier research related to salt transport in estuaries with significant gravitational circulation suggests that up-estuary salt transport increases during low tidal ranges as a result of increased gravitational circulation. In the CFRE, in contrast, net (tidally averaged) near-bottom along-channel velocities are greater during higher tidal range conditions than during lower tidal range conditions. Findings indicate stronger tidal forcing and associated mixing contribute to greater near-bottom salinity gradients and, consequently, increased baroclinic circulation. Lower near-bottom salinities during the higher tidal range period are a result of a combination of increased vertical turbulent salt fluxes near the pycnocline and increased bottom-generated mixing.

Citation: Becker, M. L., R. A. Luettich Jr., and H. Seim (2009), Effects of intratidal and tidal range variability on circulation and salinity structure in the Cape Fear River Estuary, North Carolina, *J. Geophys. Res.*, *114*, C04006, doi:10.1029/2008JC004972.

1. Introduction

[2] Physical mechanisms that determine transport of constituents can strongly influence the water quality and ecologic health of an estuarine system. Temporal and spatial changes in mixing, stratification, and residual circulation can impact the spatial distribution of dissolved oxygen, pollutants, and nutrients. In a partially mixed estuary, periodic fluctuations associated with tidal currents can contribute to variations in turbulence and consequent changes in the stability of the water column. Evidence of the impact of tidal range (spring-neap) and intratidal (flood-ebb) variability on circulation and salt transport has been found in results of observational and theoretical studies. Laboratory experiments and observations in a number of estuaries, for example, suggest estuarine gravitational circulation and associated up-estuary salt transport can strengthen during periods of reduced tidal forcing, such as during the neap tide [*Linden and Simpson*, 1988; *Monismith et al.*, 1996; *Stacey et al.*, 2001; *Bowen and Geyer*, 2003]. Asymmetries associated with strain induced periodic stratification resulting in increased stratification (and greater stability) during the ebb tide and the reverse effect during the flood have also been found to significantly influence the strength of residual circulation [*Monismith et al.*, 1996; *Stacey et al.*, 2001]. Research suggests that mixing, circulation, and salt transport characteristics are closely linked to periodic fluctuations in the strength of turbulence and stratification which often vary on tidal timescales [*Jay and Smith*, 1990a; *Rippeth et al.*, 2001; *Stacey et al.*, 2001; *Stacey and Ralston*, 2005].

[3] Understanding the relationship between turbulent mixing and stratification is a key component to accurately depicting the strength of estuarine circulation and the associated transport. Classical models for rectangular channels [e.g., *Hansen and Rattray*, 1965, 1966] were based on tidally averaged conditions and led to stratification-circulation diagrams that depict the relationship between estuarine circulation and the vertical salinity structure. On the basis of velocity and salinity measurements, estuaries could be classified into different types ranging from diffusion-dominated (analogous to well-mixed) estuaries with little or no gravitational estuarine bottom flow on one end of the spectrum to more strongly stratified (analogous to salt wedge) estuaries in

[1]Department of Marine Sciences, University of North Carolina at Chapel Hill, Chapel Hill, North Carolina, USA.
[2]Institute of Marine Sciences, Morehead City, North Carolina, USA.

0148-0227/09/2008JC004972

which gravitational (''estuarine'') circulation is significant and the estuary more closely resembles a two-layer system. In classical estuarine circulation models, upstream salt transport is represented by a combination of density-driven flow (''estuarine gravitational'' or ''residual'' salt flux) and tidal diffusion. For steady state conditions, these fluxes balance the downstream transport of salt [*Hansen and Rattray*, 1965; *Simpson et al.*, 2001].

[4] Observational studies in tidally energetic systems have considered how variability in tidal forcing influences (estuarine gravitational and diffusive) salt transport characteristics. Research indicates that in the Columbia River Estuary, for example, salt primarily enters the estuary as a result of tidally driven transport near middepth. The behavior is believed to be associated with internal wave motion and was found to increase during periods of strong stratification [*Jay and Smith*, 1990b]. In the Hudson River Estuary, in contrast, tidally driven (oscillatory) salt transport is reported to be a relatively minor component of the salt balance. Most of the salt entering the estuary was found to be associated with estuarine gravitational transport during monthly (''apogean'') neap tides when increased landward movement of salt occurred [*Bowen and Geyer*, 2003]. Patterns of increased estuarine circulation and salt transport during neap tides have also been observed by other researchers [*Nunes and Lennon*, 1987; *Monismith et al.*, 1996; *Blanton et al.*, 2003], and results of lab experiments suggest baroclinic circulation diminishes during periods of increased turbulence [*Linden and Simpson*, 1988]. *Blanton et al.* [2003], for example, found increased up-estuary import of salt in the Satilla River Estuary occurred at depth during the neap tide, a trend consistent with enhanced gravitational circulation. The observed pattern of decreased gravitational circulation during higher tidal range periods has been attributed to increased vertical mixing that weakens the baroclinic flow. During periods of increased stratification such as during the neap tide, in contrast, tidal mixing may be inhibited, and baroclinic circulation can strengthen [*Monismith et al.*, 1996; *Li et al.*, 1998; *Stacey et al.*, 2001].

[5] While increased vertical mixing may directly *weaken* circulation (as a result of increased vertical exchange of momentum), stronger vertical mixing can increase the horizontal salinity gradient and consequently *strengthen* density-driven circulation. The effects of the two opposing influences on estuarine circulation have been considered on the basis of parameters derived from simple classical models [e.g., *Hansen and Rattray*, 1965; *Prandle*, 1985] and mechanical energy considerations. *Park and Kuo* [1996] developed diagnostic ratios based on fractional changes in horizontal salinity gradients and mixing (expressed via vertical eddy viscosity coefficient, A_z, or tidal current amplitude) to predict effects on residual circulation. As mixing increases, if the dimensionless ratio of the fractional change in the horizontal salinity gradient to the fractional change in tidal current amplitude is greater (less) than unity, gravitational circulation is expected to increase (decrease). Similarly, *Weisberg and Zheng* [2003] considered sources and sinks of mechanical energy and numerical model results to investigate how changes in mixing can influence estuarine circulation. Results showed that if ratios of work associated with buoyancy to work associated with turbulent production increased (decreased), estuarine circulation would be expected to strengthen (diminish). The conditions supporting these two opposing cases have been considered primarily in numerical modeling studies [*Park and Kuo*, 1996; *Weisberg and Zheng*, 2003].

[6] Additional research in stratification-circulation relationships has addressed the effects of changes in mixing and stratification throughout the water column including variability on intratidal timescales [*Simpson et al.*, 1990; *Jay*, 1991; *Monismith et al.*, 1996; *Nepf and Geyer*, 1996]. Observations provide evidence that variability in the strength of residual circulation is intimately linked to flood-ebb asymmetry in stratification [*Monismith et al.*, 1996; *Stacey et al.*, 2001] in addition to neap-spring cycling. During the ebb tide, for example, tidal straining can act to stratify the water column, and increased baroclinic circulation can develop [*Monismith et al.*, 1996].

[7] Other research has considered the effects of lateral variations on estuarine dynamics including influences on residual circulation and salt balances [*Fischer*, 1972; *Dyer*, 1974; *Wong*, 1994; *Li et al.*, 1998]. As the strength of baroclinic circulation depends on depth, for example, results of observational and theoretical studies indicate up-estuary flow tends to be concentrated in the channel and seaward flow tends to occur across the shoals [*Wong*, 1994; *Li et al.*, 1998].

[8] In this research, we investigate the influence of tidal range and intratidal variations on the along-channel circulation and the salinity structure in the largely unstudied Cape Fear River Estuary (CFRE), a partially mixed estuary along the southeast coast of the United States (Figure 1). We seek to gain insight on how tidal range variability influences salinity characteristics during low river flow conditions. Analysis of historical data (Figure 2) during periods of low river inflow (<65 m s^{-1}) suggests tidal range, stratification, and near-bottom salinities are critically linked and vary according to a 29-day modulation. An inverse relationship between tidal range and stratification or tidal range and near-bottom salinity exists during the low river inflow period.

[9] These relationships are explored more closely using data collected during a field experiment designed to capture hydrodynamic and salinity variations for two different tidal range periods (i.e., conditions representing low versus higher ranges during periods when river flow is low and relatively constant). We compare along-channel circulation and salinity characteristics, calculated baroclinic accelerations, and tidally driven and mean advective horizontal salt fluxes for the two tidal range periods. We then discuss differences in the vertical mixing structure through comparison of turbulent vertical salt fluxes and coefficients of vertical eddy diffusivity for salt based on [*Munk and Anderson*, 1948] parameterizations and those computed from a simplified salt budget equation. Finally, we discuss how tidal range differences impact mixing, stratification, residual circulation, and salt transport characteristics and how these relate to previous studies.

2. Study Area

[10] The CFRE (Figure 1) is a funnel-shaped, partially mixed to well mixed (near the mouth) estuary in which river flow and tidal currents can strongly influence hydrodynamic conditions. The estuary is dominated by semidiurnal tides

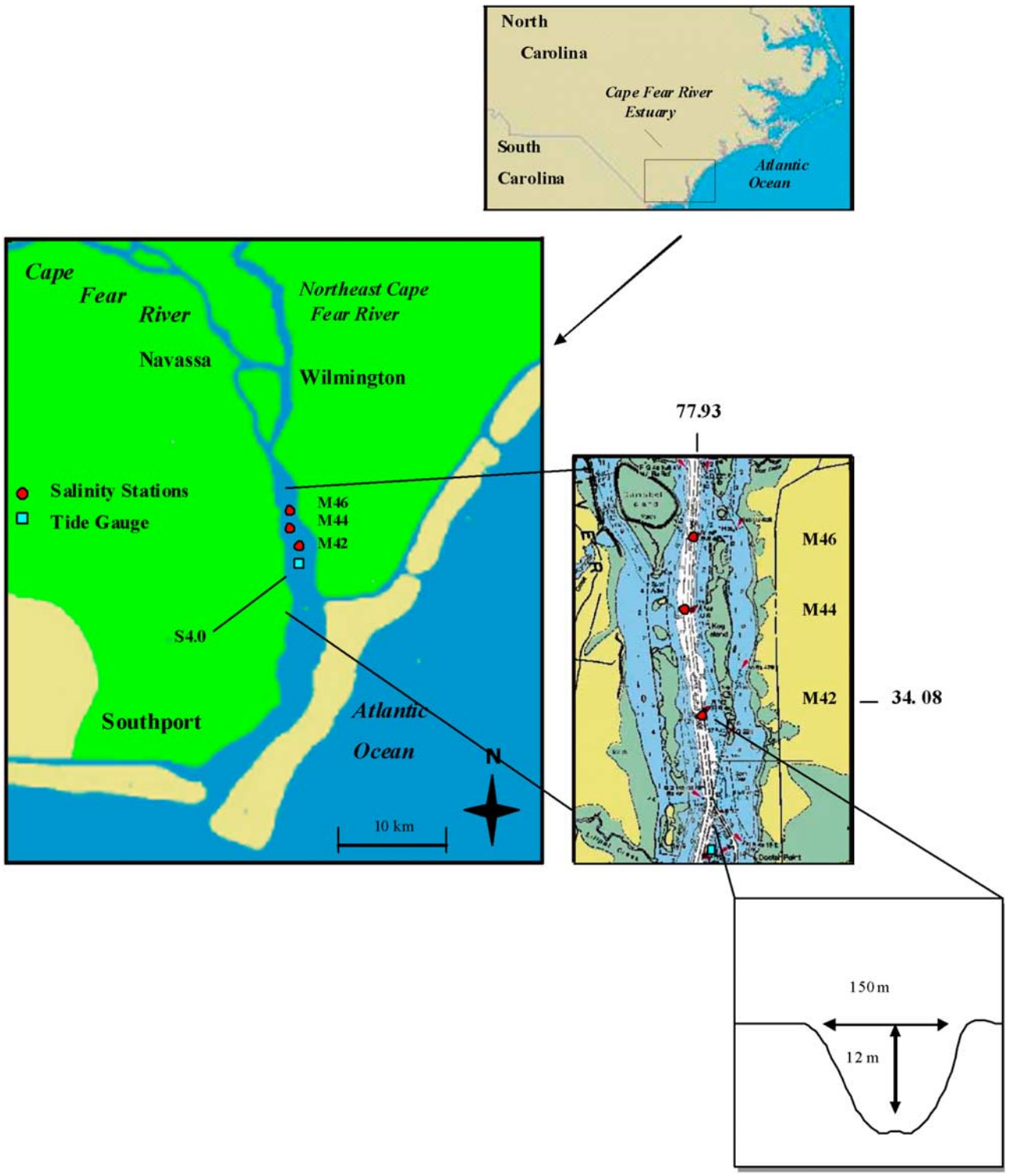

Figure 1. Cape Fear River Estuary field study area including field survey stations and charted channel.

(M_2, N_2, and S_2) with about 85% of the amplitude attributable to the three largest constituents [*Welch and Parker*, 1979; *Becker*, 2007].

[11] The CFRE is approximately 1800 m wide at the mouth and narrows to a width of about 180 m near Wilmington. A navigation channel is maintained from close to the mouth of the estuary near the Atlantic Ocean to near Navassa, a distance of approximately 50 km. Depths in the main channel are maintained to a minimum depth of 11.6 m and width of approximately 150 m [*McAdory*, 2000]. Outside of the main channel, tidal marshes occupy parts of the estuary, while shoals and spoil areas typically reach depths of ~0.3 to ~5 m.

[12] The Cape Fear River accounts for approximately 60% of freshwater flow into the CFRE. Flow from two smaller coastal plain rivers, the Northeast Cape Fear River

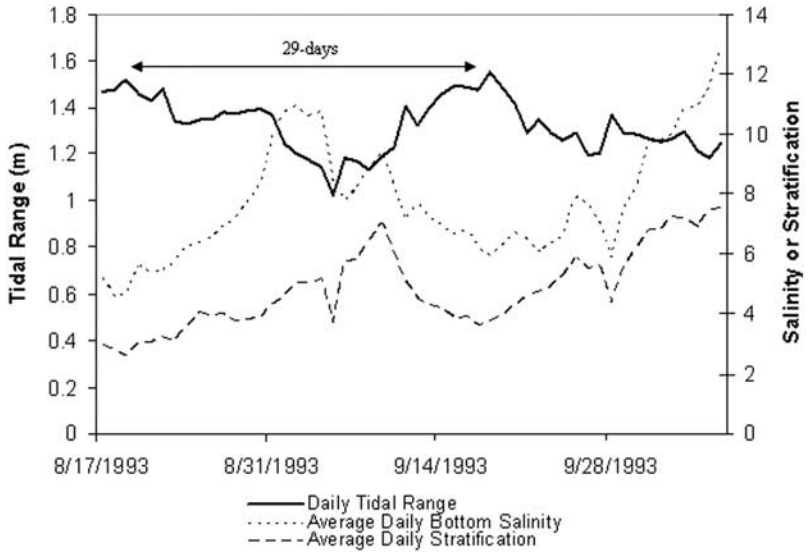

Figure 2. Relationship between tidal range, near-bottom salinity, and stratification based on historical (1993) data.

and the Black River, also contribute to the amount of freshwater entering the estuary, particularly during moderate to high-flow conditions. River flow from the Cape Fear River is highly variable with low-flow discharge (<100 m^3 s^{-1}) generally characteristic of summer conditions and greater freshwater inflow (~300–600 m^3 s^{-1}) more typical of spring and winter conditions. Very high discharge events of greater than 1100 m^3 s^{-1} have been observed with a recurrence interval of about 4 years based on a 32-year peak flow record.

[13] In the present study we examine tidal range and salinity characteristics during conditions of low freshwater flow (<75 m^3 s^{-1}) when the salinity intrusion is expected to be in its base flow (low-flow) position.

3. Methods: Experimental Design

[14] In order to characterize the salinity and velocity structure in the central CFRE during low versus higher tidal range conditions, a field study that included the collection of tidal height, velocity, and salinity data was conducted in the summer of 2005. Velocity and salinity data were collected throughout the tidal cycle on 12 July 2005 and 26 July 2005, representing low and higher tidal ranges, respectively, using a vessel-mounted ADCP (for velocities) and CTD sampling instruments (for salinities).

3.1. Setting and Physical Conditions

[15] The field study area consisted of an approximately 2.8 km, relatively straight, along-channel section near midestuary (Figure 1). The section coincides with a location approximately midway between the estuarine mouth and the limit of salinity intrusion for low to average river flow conditions [*Becker*, 2007].

[16] Examination of the hydrograph of mean daily discharge on the Cape Fear River from 29 June to 7 August indicates peaks in river discharge within a 12-day window prior to sampling reach only 73 m^3 s^{-1} prior to the 12 July sampling day and 67 m^3 s^{-1} prior to the 26 July date, consistent with low-flow conditions in each case [*Becker*, 2007].

[17] Winds during the two sampling dates were generally light. Winds during the 12 July sampling period (~0800 to 2200 LT), based on hourly measurements at Wilmington, were generally from the south or southwest with an average wind speed of 2.9 m s^{-1} and recorded maximum value of 6.2 m s^{-1}. On 26 July, the wind direction was generally from the north or northwest during the daytime sampling (~0800 to 1800 LT) and generally calm or variable in the evening. The average recorded wind speed was 2.1 m s^{-1} with recorded speeds not exceeding 3.6 m s^{-1}.

3.2. Data Collection: Water Level, Velocity, and Salinity Measurements

[18] A water level gauge was installed at a location near midestuary (S4.0, Figure 1). Water level values were recorded every 30 min from 29 June through 7 August. Velocities were measured using a vessel-mounted, 1200 kHz Acoustic Doppler Current Profiler (R.D. Instruments Workhorse ADCP) from the vicinity of Channel Marker 42 to the vicinity of Channel Marker 46 (along-channel, downstream-to-upstream transects spanning a distance of approximately 2.8 km). Velocities were measured from near surface to near bottom in 1-m increments. Values were recorded every 3 s and later averaged to represent 5-min intervals. Sampling continued throughout the tidal cycle each day in order to obtain data representing flood, ebb, and slack tides.

[19] Salinities in the main channel were measured throughout the water column at Markers 42, 44, and 46 (Figure 1). The salinity data were collected by lowering recording instruments (Hydrolab and YSI CTDs) from near surface to near bottom in 1-m increments from sampling vessels. One vessel was generally stationed at M44 throughout each measurement period (with the exception of after-sunset/evening sampling). Measurements at other stations were conducted in conjunction with velocity measurements. Salinity sampling was conducted in collaboration with the NC State Division of Water Quality Intensive Survey Unit.

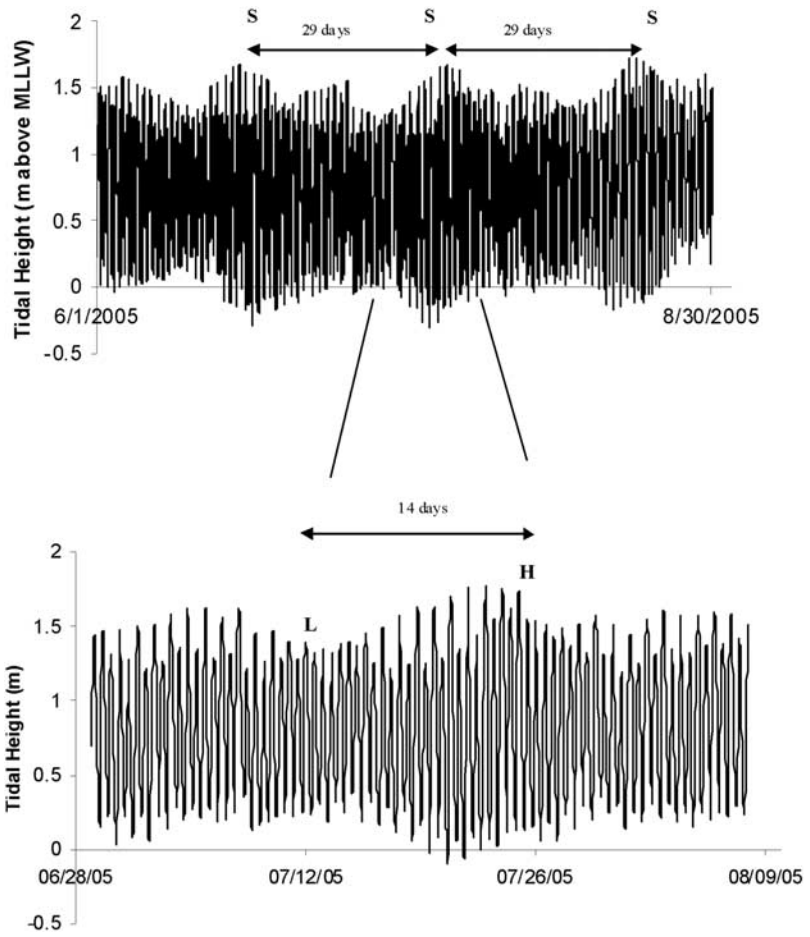

Figure 3. Measured tidal heights at (top) Wilmington tide gauge and (bottom) field data station S4.0. "S" indicates times of particularly large spring tides. "L" (low) and "H" (high) indicate differences in tidal ranges for the 12 July and 26 July sampling periods.

[20] The spatial resolution of the data collection study (i.e., salinity sampling at locations ~700 to ~1400 m apart over the total range of ~2.8 km) was designed to provide a reasonable representation of the along-channel salinity field while being able to complete transects quickly enough so that each part of the tidal cycle would be well represented. The magnitude of the along-estuary salinity gradient in this part of the CFRE, based on analysis of vertical salinity sections, typically varies from about 0.6 to 1.2 km^{-1} depending on river inflow. Values as low as ~0.4 km^{-1} and as high as ~1.8 km^{-1} in the middle to lower estuary have been observed [*Becker*, 2007].

[21] In order to estimate the appropriate vertical resolution for obtaining salinity data, vertical profiles from a United States Army Corps of Engineers field study [*Benson and Parmen*, 1995] were reviewed. Analysis of these salinity data suggested vertical salinity gradients in the proposed study area are typically from 0.3 to 0.7 m^{-1}.

4. Results

4.1. Tidal Elevations and Velocity Transects

[22] Measured tidal elevations at Wilmington and S4.0 during the summer 2005 study period indicate a 29-day modulation of the predominantly semidiurnal tidal signal (Figure 3). Tidal ranges during the two field study periods were approximately 1.0 m on 12 July and 1.4 m on 26 July.

[23] Effects of wind on water level (sea level setup) were considered on the basis of low-pass filtered (30-h) times series of field data collected in this study and historical data [*Becker*, 2007]. During periods of low observed winds occurring during the field study, the analysis suggests water level was not significantly impacted by the weak wind activity. On the basis of scale analysis [*Wong*, 1994], estimated remote wind-driven circulation was 0.002 m s^{-1} (12 July) and −0.004 m s^{-1} (26 July). Estimated local wind-driven circulation was 0.005 m s^{-1} to 0.03 m s^{-1} (12 July, assuming A_z = 0.003 m^2 s^{-1} to 0.02 m^2 s^{-1}) and −0.001 m s^{-1} to −0.005 m s^{-1} (26 July, assuming A_z = 0.006 m^2 s^{-1} to 0.03 m^2 s^{-1}) [*Prandle*, 1985; *Wong*, 1994; *Dyer*, 1997]. Transect- and depth-averaged along-channel velocities and tidal heights at S4.0 are given in Figure 4. The maximum transect-averaged velocities reached 0.63 m s^{-1} during the flood tide and 0.62 m s^{-1} during the ebb tide on 12 July and 0.86 m s^{-1} during the flood tide and 0.78 m s^{-1} during the ebb tide on 26 July.

[24] A total of thirteen velocity transects (numbered "0" to "12," Figure 5) were measured on 12 July, and a total of nineteen transects (numbered "0" to "18") were recorded on 26 July. Time represents the number of hours into

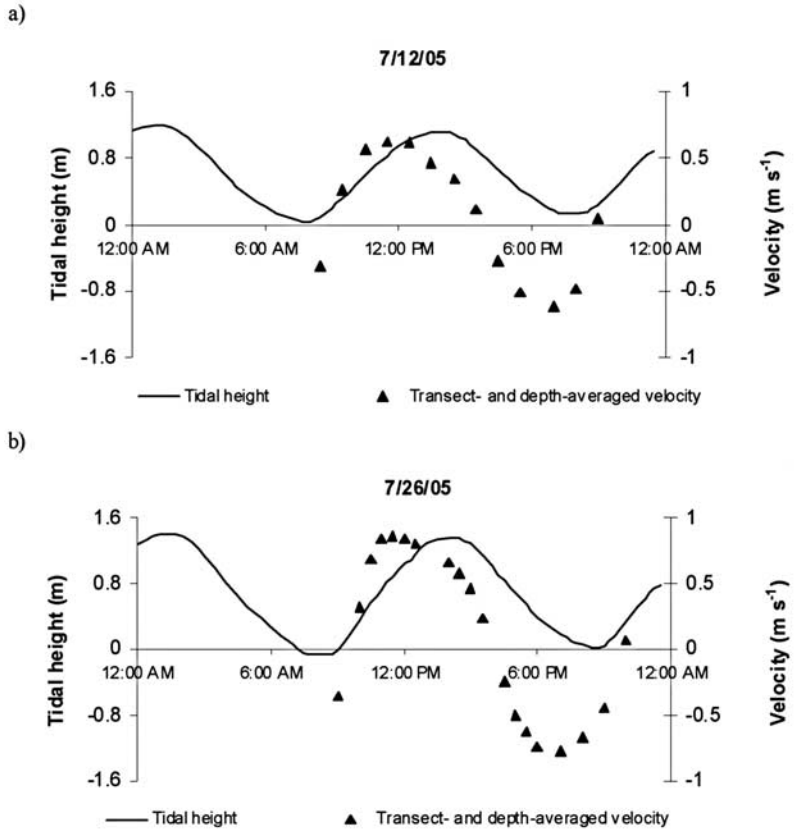

Figure 4. Tidal height at S4.0 and depth-averaged along-channel velocity on (a) 12 July and (b) 26 July 2005.

sampling (where $t = 0$ represents the sampling time at the midpoint of Transect 0).

[25] The first transect (Transect 0) on each sampling day (Figure 5) represented a period close to low tidal elevation when the tide was still ebbing. Transect 1 on each day illustrates the development of the flood tide near the bottom of the water column. Transect 4 profiles show the velocity structure near maximum flood tide conditions, during which the velocity maximum occurs at approximately 4 m below the surface on each sampling day. Transect 8 on 12 July and Transect 11 on 26 July show the beginning of the ebb tide with stronger velocities apparent near the top of the water column. Final transects of each day, Transects 12 (12 July) and 18 (26 July), display the velocity profiles near slack tide, a time when the velocity structure resembles that of a two-layer system in which outflow occurs near the surface and inflow is observed near the bottom. Along-channel velocities near slack tide are similar in magnitude near the bottom ($\sim$0.29 m s^{-1} versus 0.33 m s^{-1} at $\sim$12 m depth for low and higher tidal range conditions, respectively).

4.2. Density, Stratification, and Salinity Characteristics

[26] The density structure during each study period was primarily influenced by salinity, as water temperatures were relatively constant (typically less than 1°C variation). Densities at M44 on each sampling day ranged from $\sim$1007 kg m^{-3} to $\sim$1015 kg m^{-3}.

[27] Salinity stratification, measured as the near-surface to near-bottom salinity difference at M44, and tidal height are shown in Figure 6. During low tidal range conditions, stratification ranged from about 7 to 9 and showed relatively little variability with ebb and flood cycles. During the higher tidal range period, in contrast, stratification ranged from less than 5 to about 10, with increases generally observed during the ebb tide and decreases during the flood tide. Similar patterns were observed at M42 and M46.

[28] Vertical buoyancy frequencies (N) were calculated according to

$$N^2 = \frac{-g}{\rho_0}\frac{\partial \rho}{\partial z} = (\text{vertical buoyancy frequency})^2, \qquad (1)$$

where g is gravitational acceleration, ρ is density, ρ_o is constant reference density, and z is depth. Depth-averaged buoyancy frequencies (N) and depth-averaged, transect-averaged, along-channel velocities are shown in Figure 7. During low tidal range conditions, buoyancy frequencies remain at a relatively constant value of $\sim$0.07–0.08 s^{-1} (with the exception of a dip in values to $\sim$0.06 s^{-1} between $\sim$1130 and 1330 LT, when velocities were close to the flood tide maximum and when observed wind stress toward the north reached a maximum of $\sim 3.4 \times 10^{-2}$ Pa at 1253 LT based on quadratic wind stress relationships, $C_d = 1.14 \times 10^{-3}$). During higher tidal range conditions, the buoyancy frequencies ranged from about 0.05 s^{-1} to 0.08 s^{-1}, with lower values generally occurring during the flood tide.

[29] Buoyancy frequency squared (N^2) and salinity contours throughout the water column at M44 are shown

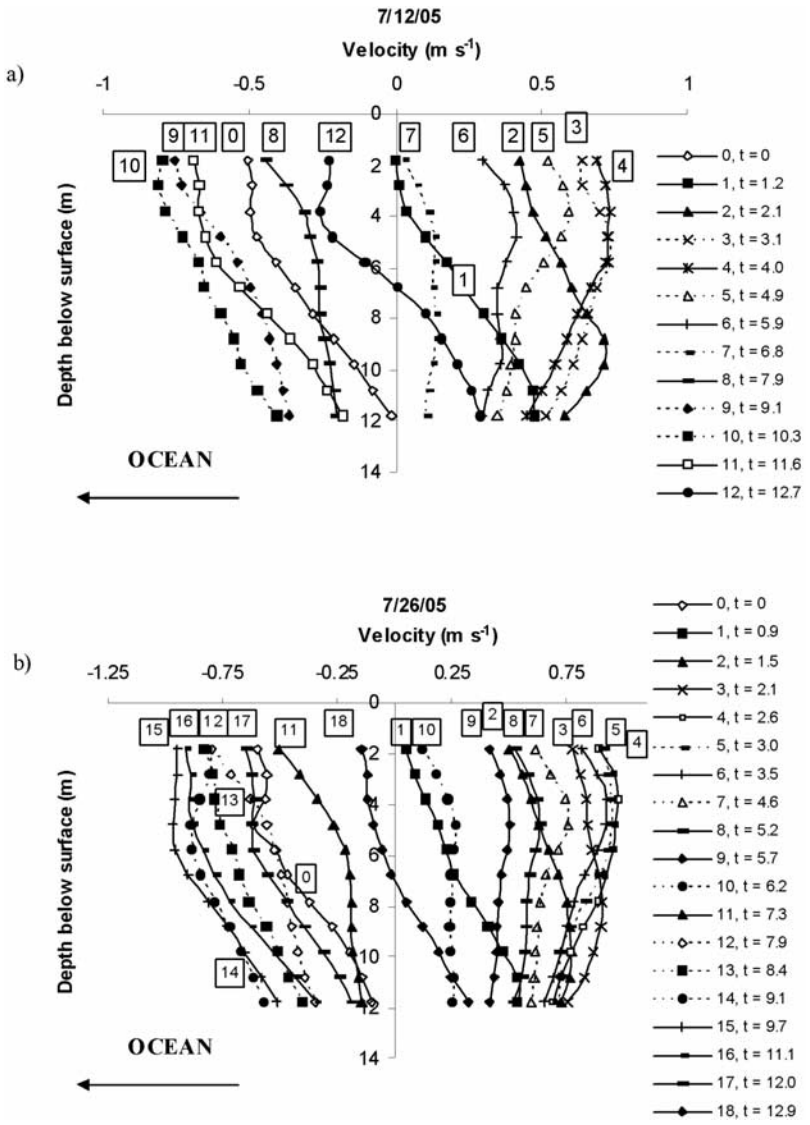

Figure 5. Along-channel velocities on (a) 12 July and (b) 26 July. Times (t) represent the number of hours into sampling (where $t = 0$ represents the sampling time at the midpoint of the first transect).

together in Figure 8. Times of maximum flood ("F_{max}") and maximum ebb ("E_{max}") velocities are labeled. Maximum, tidally averaged N^2 values occur at a depth of ~5 m below surface for both tidal range periods.

[30] Salinity profiles at M44 are shown in Figure 9. On 12 July, near-bottom salinity increased from ~18 near slack tide to ~21 near the end of the flood tide and then fell during the ebb tide from ~21 to ~19 near slack after ebb (Figure 9a). On 26 July (Figure 9b), in contrast, near bottom salinity increased from ~16 during slack to ~21 near the end of the flood tide and then fell back to ~16 near slack after ebb. Near-bottom salinities at the end of the flood tide reached similar values (~21) for both low and higher tidal range conditions (with a greater slack to max-flood range on 26 July). By the end of the ebb on 12 July, salinities remained higher than at the start of the tidal cycle (and higher than on 26 July), whereas at the end of the ebb on 26 July, near-bottom salinities were close to their values at the beginning of the cycle (Figure 9c). Similar patterns of increased near-bottom salinities during the low tidal range period were observed at M42 and M46.

5. Analysis

5.1. Tidally Averaged Velocities, Salinities, and Salt Fluxes

[31] Tidally averaged velocity profiles (Figure 10a), computed from the transect-averaged velocities, reveal a similar structure for both 12 July and 26 July. Velocities reach ~−0.1 m s^{-1} near the surface and ~0.1 m s^{-1} (12 July) to ~0.15 m s^{-1} (26 July) near the bottom. On 26 July, a marked increase in tidally averaged velocities exists in the lower portion of the water column (below ~9 m below surface). We note that findings suggest (remote and local) wind-driven circulation in the CFRE is small relative to (at least an order of magnitude less than) observed tidally averaged (near-bottom) velocities.

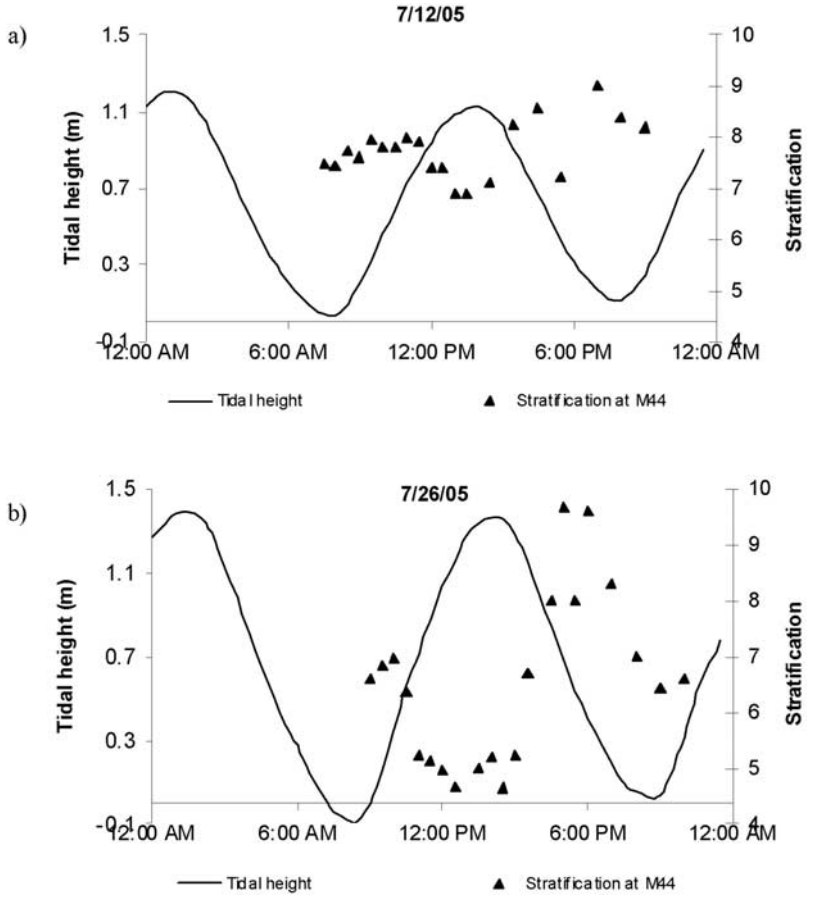

Figure 6. Salinity stratification and tidal height at M44 on (a) 12 July and (b) 26 July.

[32] Tidally averaged salinity profiles (Figure 10b) indicate near-surface salinities reach ~12 (with slightly greater values on 26 July) and ~18 to ~20 near the bottom (with salinities consistently greater on 12 July in the portion of the water column below ~2 m below surface). Depth-averaged, tidally averaged horizontal salinity gradients, calculated from salinity measurements at M42 and M46, were -0.5 km^{-1} on 12 July and -0.6 km^{-1} on 26 July.

[33] Baroclinic acceleration, a_b, may be computed according to

$$a_b(z) = -\frac{g}{\rho}\int_z^{\eta}\frac{\partial \rho}{\partial x}dz \tag{2}$$

where η is sea surface elevation and x is along-channel distance [*Dyer*, 1997].

[34] A finite difference integration from near-surface to depth was performed on the basis of salinity data at M42 and M44. Results (Figure 10c) indicate the calculated accelerations on 26 July exceed those on 12 July at each depth. A notable increase in the difference between baroclinic acceleration during the two sampling periods exists at depth (~9–12 m below surface). This increase results from increased horizontal salinity gradients in the lower water column during the higher tidal range period (i.e., approximately -0.6 km^{-1} on 26 July versus -0.4 km^{-1} on 12 July).

[35] On the basis of a simple salt flux equation, the total flux of salt at a particular along-channel location was calculated as a function of depth according to

$$(\overline{us}) = (\overline{u})(\overline{s}) + \overline{u_t s_t} \tag{3}$$

where u is along-channel velocity, s is salinity, the overbar represents a time average over a tidal cycle, and the subscript t denotes tidal variations. The term on the left represents the total salt flux. The first term on the right represents the mean advective (or residual) flow. The last term represents fluxes associated with time-varying processes often linked to tidal effects and may include contributions from a number of dispersive fluxes [*Kjerfve*, 1986; *Jay and Smith*, 1990b]. Along-channel upstream salt fluxes (Figures 10d and 10e), calculated from equation (3) from the velocities and the salinities at M44, indicate transport is dominated by mean advection in the lower portion of the water column and by tidal processes around middepth. Maximum tidally driven fluxes occur at ~5 m below surface and reach 0.89 to 1.1 m s^{-1} (with greater values during the higher tidal range period). Maximum up-estuary mean advective salt fluxes occur near the bottom and are ~2–3 m s^{-1}.

[36] Tidally and depth-averaged (from ~2 m below surface to near bottom) total salt fluxes were ~0.8 m s^{-1} (upstream) on 12 July and ~1 m s^{-1} on 26 July. Tidally and depth-averaged mean advective salt fluxes were 0.48 m s^{-1} on 12 July and 0.51 m s^{-1} on 26 July.

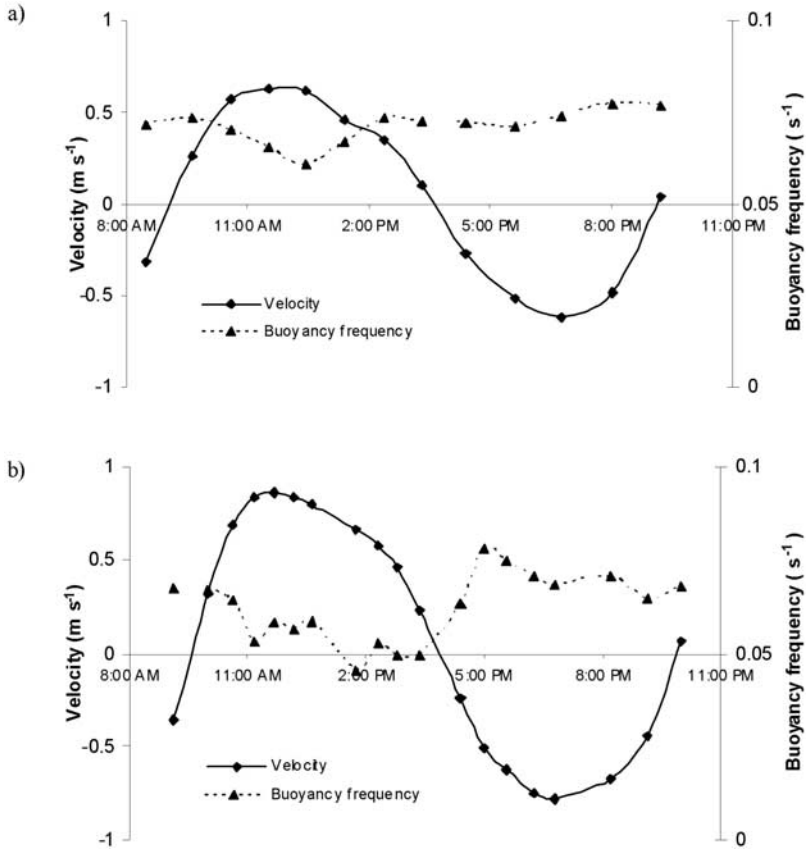

Figure 7. Transect- and depth-averaged along-channel velocities and depth-averaged buoyancy frequencies at M44 on (a) 12 July and (b) 26 July.

5.2. Tidal Oscillations in Velocity and Salinity

[37] Tidal fluctuations in velocity and salinity at a particular depth and along-channel location were examined using a simple model based on harmonic representations:

$$\hat{u}_t = U_o \cos(\omega t + \phi_u) \tag{4}$$

$$\hat{s}_t = S_o \cos(\omega t + \phi_s) \tag{5}$$

where $\hat{u}_t$ is deviation from the tidally averaged along-channel velocity, $\hat{s}_t$ is deviation from the tidally averaged salinity, U_o is amplitude of the along-channel tidal velocity variation, S_o is amplitude of the tidal salinity variation, t is time, $\omega = \frac{2\pi}{T}$ is circular frequency, T is semidiurnal tidal period, ϕ_s is phase of the tidal salinity variation relative to low tide, and ϕ_u is phase of the along-channel tidal velocity variation relative to low tide [*Officer*, 1976; *Dyer*, 1997].

[38] Observed values of $\hat{u}_t$ were determined for different parts of the tidal cycle (such that the time periods between sampling were approximately equal) by subtracting measured values of the transect-averaged along-channel velocity from the tidally averaged values for the low and high tidal range periods. Observed values of $\hat{s}_t$ were similarly determined by subtracting measured values of salinity at M44 from the tidally averaged values. Cosine functions (Figure 11) were fit to the observed values of $\hat{u}_t$ and $\hat{s}_t$. The start of the time series ($t = 0$) represented the time of measured low tide at S4.0 for each tidal range period. Amplitudes of tidal velocity variations (U_o) and salinity variations (S_o) were computed on the basis of the maximum and minimum observed values of $\hat{u}_t$ and $\hat{s}_t$ during the low and higher tidal range periods. T represented the time period from velocity slack after ebb to slack after flood tide for each tidal range period. Predicted values of $\hat{u}_t$ and $\hat{s}_t$ based on equations (4) and (5) were computed every 100 s. For each depth, values of ϕ_u and ϕ_s were determined by minimizing root mean squared errors (RMS) between observed and predicted values of $\hat{u}_t$ and $\hat{s}_t$.

[39] Observed and predicted values of $\hat{u}_t$ and $\hat{s}_t$ at 2 m, 5 m, and 12 m below surface together with observed tidal heights at S4.0 are shown in Figure 11. Amplitudes U_o and S_o and phase differences between tidally varying velocities and salinities, $(\phi_u - \phi_s)$ at each depth are shown in Figure 12. Amplitudes U_o and S_o were greater during the higher tidal range period at each depth. Maximum values occurred near middepth (~4–6 m below surface) during both sampling periods. Phase differences $(\phi_u - \phi_s)$ were smallest near middepth (~5 m below surface), with lower values occurring during the lower tidal range period. During both tidal range periods, phase differences were closest to quadrature in the lower portion of the water column (Figure 12c), where tidally driven salt fluxes were minimal.

[40] At a particular depth, the average salt flux associated with tidal processes, F_t, may be computed according to

$$F_t = \frac{1}{T} \int_0^T \hat{u}_t \hat{s}_t dt \tag{6}$$

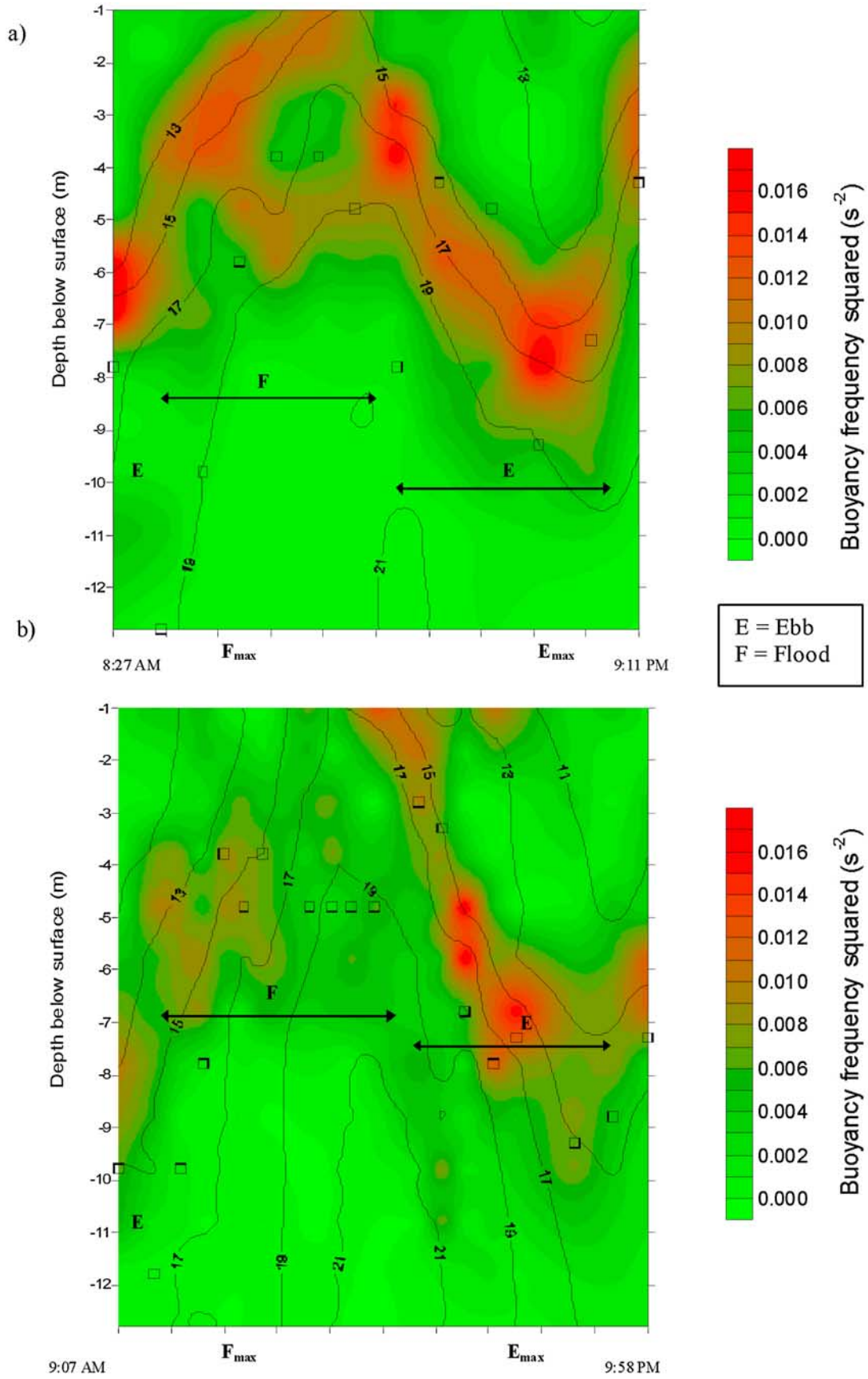

Figure 8. Buoyancy frequency squared (N^2) and salinity contours at M44 on (a) 12 July and (b) 26 July. Squares indicate the computed height of the bottom boundary layer. "F_{max}" and "E_{max}" represent times of maximum flood and ebb velocities, respectively.

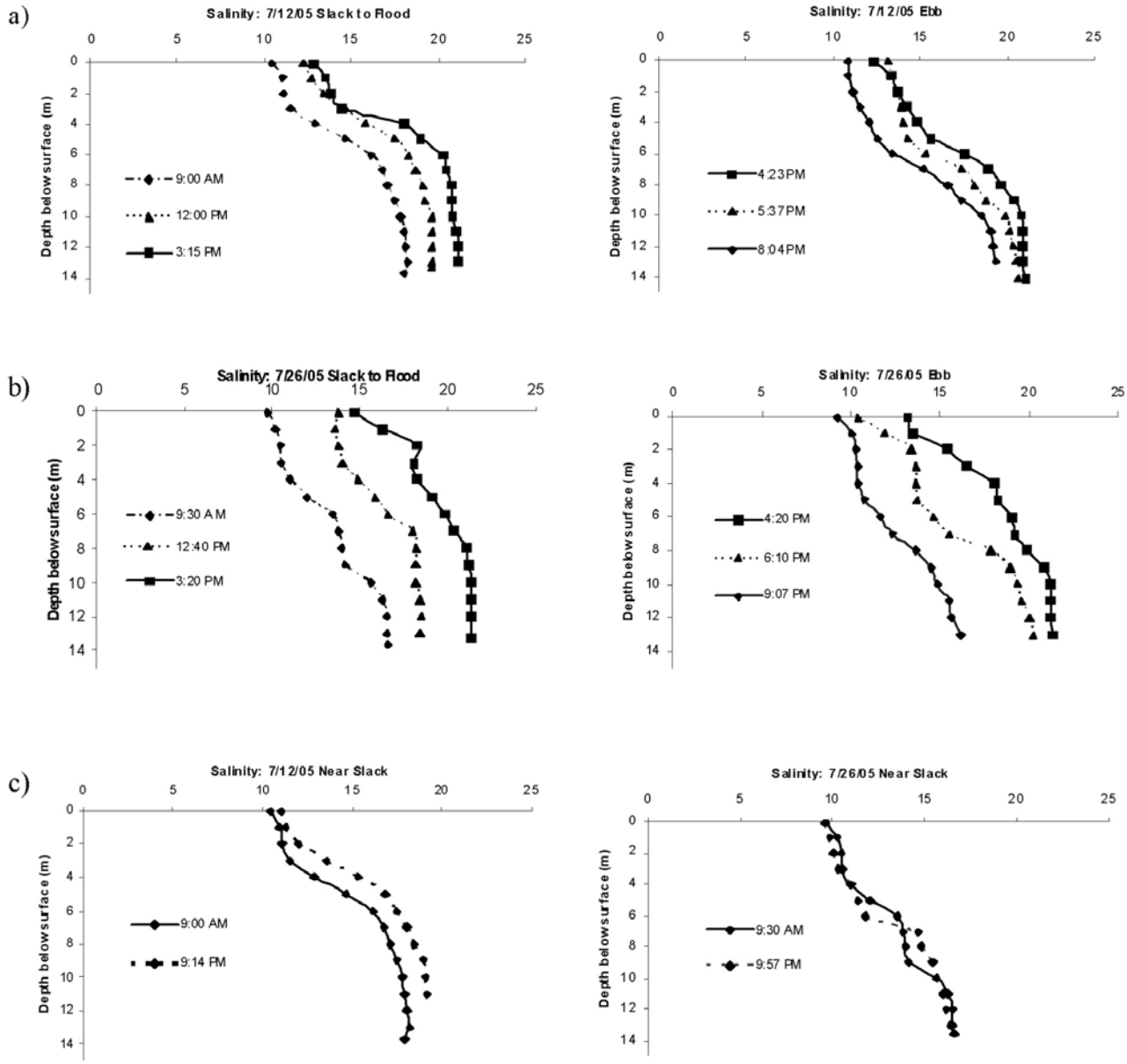

Figure 9. Salinity profiles at M44 on (a) 12 July, (b) 26 July, and (c) near slack tide on 12 July and 26 July.

A finite difference integration (with a time interval of 100 s) was performed using the predicted values of $\hat{u}_t$ and $\hat{s}_t$ from equation (4) and equation (5). A comparison of salt fluxes (F_t) calculated from equation (6) to those determined from equation (3) (term 3) (Figures 10d and 10e) is given in Table 1. Computed salt fluxes using the salt budget equation and those predicted on the basis of harmonic representations were generally in close agreement for both tidal range periods. We note the greatest deviation was observed during the higher tidal range period ~6 m below surface where turbulent mixing is significant (as discussed in sections 5.3 and 6.2).

5.3. Mixing Coefficients

[41] Coefficients of vertical eddy diffusivity for salt (K_z) throughout the water column were calculated from commonly used relationships [*Munk and Anderson*, 1948; *Nepf and Geyer*, 1996; *Dyer*, 1997]:

$$K_z = K_o\left(1 + 3.33\,Ri_g\right)^{-3/2} \tag{7}$$

where K_o is diffusivity coefficient in the absence of stratification and Ri_g is defined as

$$Ri_g = \frac{N^2}{(\partial u/\partial z)^2} \tag{8}$$

[42] In the bottom boundary layer, K_o may be represented by $K_o = \kappa u_* z$, where κ is the von Karman constant (0.4), and u_* is friction velocity. The friction velocity (u_*) may be

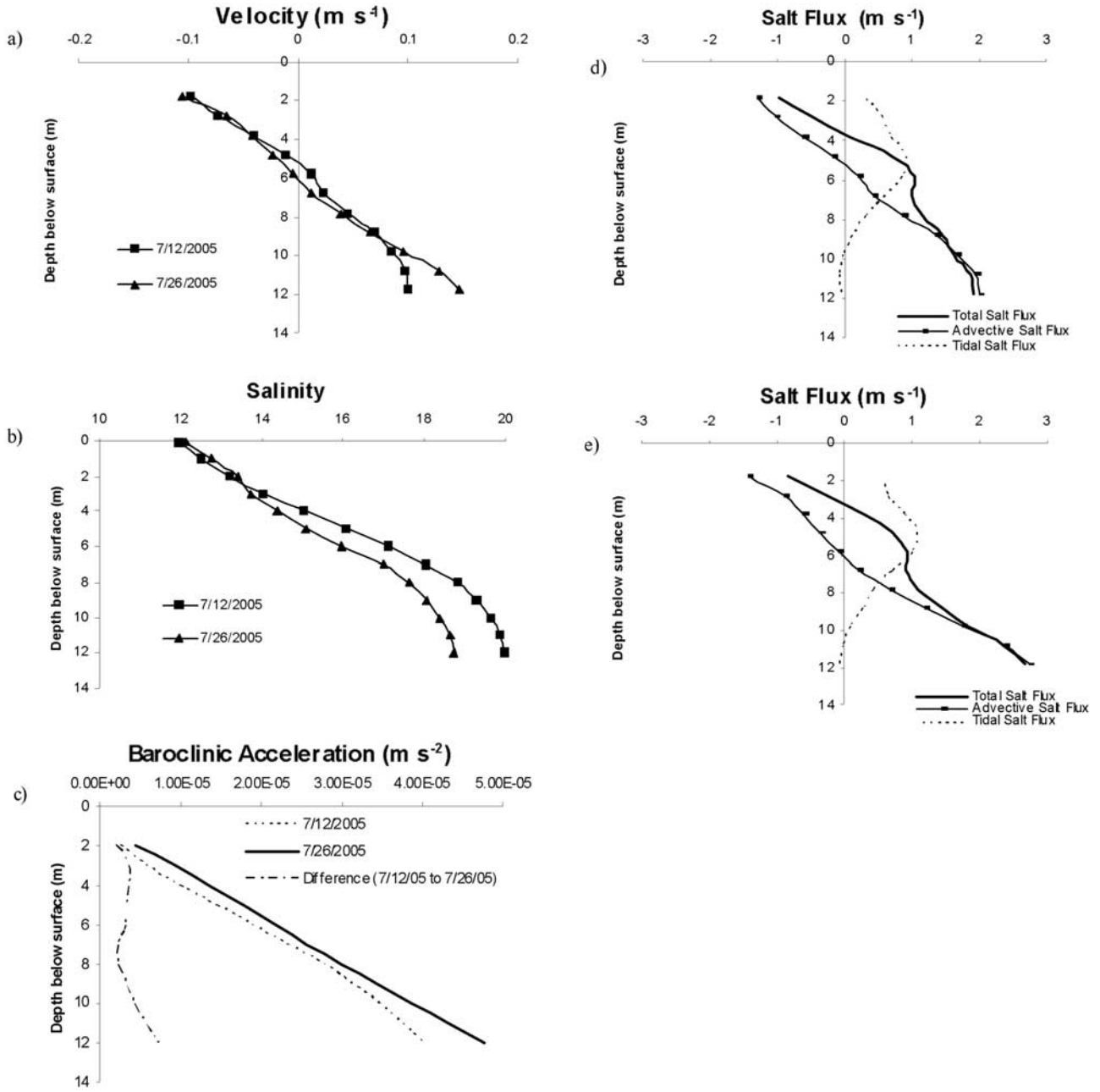

Figure 10. (a) Tidally averaged velocity on 12 July and 26 July, (b) tidally averaged salinity on 12 July and 26 July, (c) computed baroclinic acceleration on 12 July and 26 July and difference in baroclinic acceleration, (d) computed along-channel salt fluxes on 12 July, and (e) computed along-channel salt fluxes on 26 July.

represented by a quadratic friction law [*Nepf and Geyer*, 1996; *Dyer*, 1997; *Stacey and Ralston*, 2005]:

$$u_*^2 = C_d U^2 \tag{9}$$

where U is average along-channel velocity in the bottom boundary layer (BBL) and C_d is drag coefficient. Research indicates that for tidal velocities that are relatively large (e.g., $\sim$0.50 m s^{-1}), the above parameterization of u_* agrees closely with observations and that its accuracy increases at greater velocities [*Stacey and Ralston*, 2005]. During flood tide the height of the BBL corresponded to the height of the maximum along-channel velocity [*Stacey and Ralston*, 2005]. During the ebb tide, the average height of maximum shear and maximum stratification was used. The computed height of the BBL is shown by the squares in Figure 8.

[43] Gradient Richardson numbers (equation (8)) were calculated using transect-averaged along-channel velocity and salinity measurements near the midtransect location (at M44). We note that inclusion of cross-channel velocities in these calculations did not significantly affect trends, as

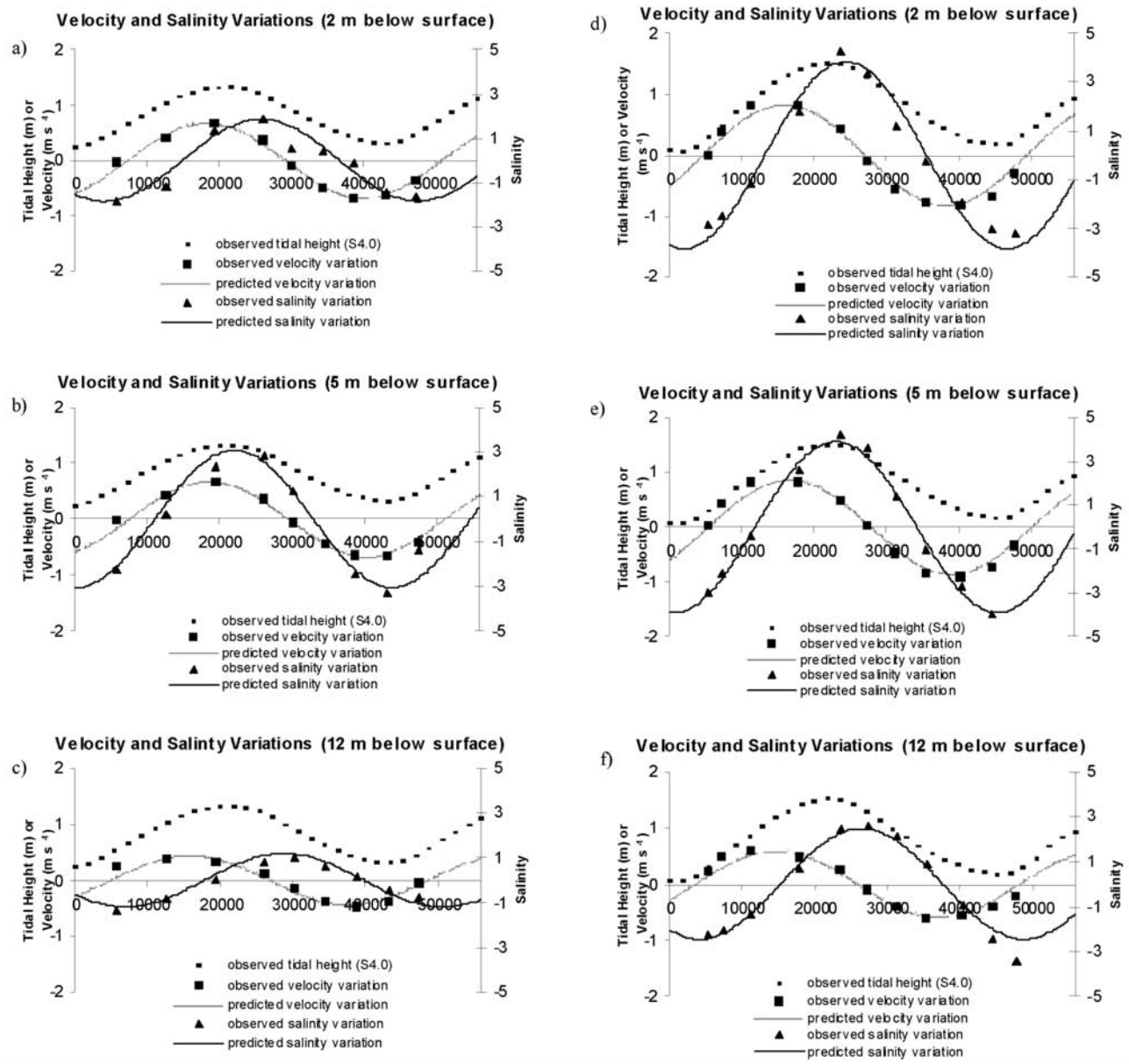

Figure 11. Tidal height, tidal velocity variations, and tidal salinity variations on (a–c) 12 July and (d–f) 26 July at 2, 5, and 12 m below surface.

cross-channel velocities were typically small relative to along-channel velocities (typically an order of magnitude less and never exceeding 0.07 m s^{-1}, the value reached near flood tide maximum during the low tidal range period).

[44] Calculated values of $Log_{10}(K_z)$ based on equation (7) with $C_d = 0.001$ together with salinity contours are shown in Figure 13. Values of $Log_{10}(K_z)$ less than -5 were ignored (not assigned a number), as these values tended to coincide with areas of very low shear (i.e., around the velocity maximum at or above the height of the BBL).

[45] Values of K_z were compared to those computed using a simple salt balance equation:

$$\frac{\partial s}{\partial t} = -u\frac{\partial s}{\partial x} + \frac{\partial}{\partial z}\left(K_z\frac{\partial s}{\partial z}\right) \tag{10}$$

where

$$\left(K_z\frac{\partial s}{\partial z}\right) = -\overline{w's'},$$

K_z is the coefficient of vertical eddy diffusivity of salt, $(\overline{w's'})$ is the vertical turbulent salt flux, and the overbar refers to a time average. Coefficients of vertical eddy diffusivity (K_z) of salt were calculated by integrating equation (10) stepwise from near bottom to each depth based on the collected salinity and transect-averaged velocity data. Negative values of K_z were ignored. Values of $Log_{10}(K_z)$, together with contours of calculated vertical turbulent salt fluxes for values greater or equal to 0.001 m s^{-1} are shown in Figure 14.

[46] Values of K_z (Figure 13) in areas of weak stratification within the BBL are in reasonably close agreement with

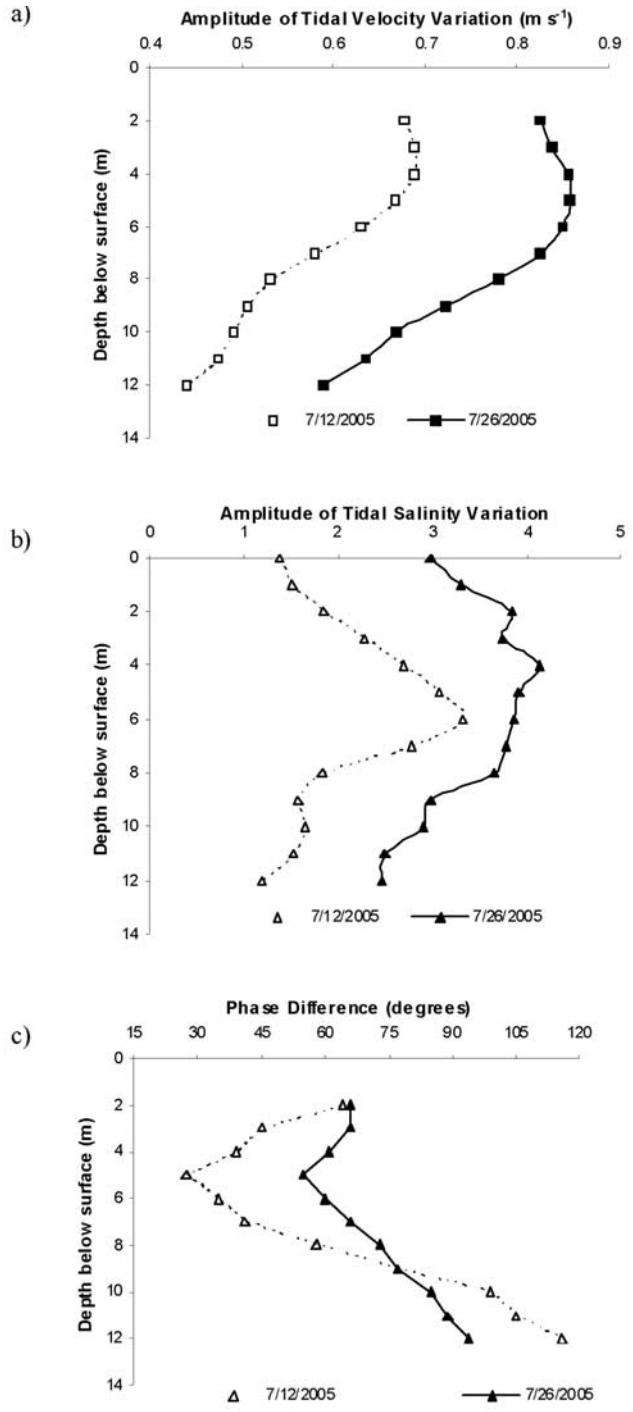

Figure 12. (a) Amplitudes of tidal velocity variations (U_o), (b) amplitudes of tidal salinity variations (S_o), and (c) phase differences between tidal velocity and tidal salinity variations.

calculated values from the salt budget equation (Figure 14). On 12 July, the values of K_z near maximum flood tide below the pycnocline reach $\sim 1 \times 10^{-2}$ to 3×10^{-2} m^2 s^{-1} (and $\sim 2 \times 10^{-2}$ m^2 s^{-1} based on the salt budget computations). On 26 July, values near maximum flood tide in the bottom part of the water column reach $\sim 1 \times 10^{-2}$ to 5×10^{-2} m^2 s^{-1} ($\sim 1 \times 10^{-2}$ m^2 s^{-1} to $\sim 9 \times 10^{-2}$ m^2 s^{-1} based on the salt budget). Near-surface values during the flood tide are $\sim 2 \times 10^{-3}$ to $\sim 1 \times 10^{-2}$ m^2 s^{-1} (and $\sim 3 \times 10^{-3}$ up to $\sim 8 \times 10^{-3}$ m^2 s^{-1} based on the salt budget).

[47] During the ebb tide on 12 July, values of K_z generally remained low in the bottom part of the water column, with typical values of $\sim 3 \times 10^{-4}$ m^2 s^{-1} (and $\sim 1 \times 10^{-4}$ to $\sim 9 \times 10^{-4}$ m^2 s^{-1} based on the salt budget). On 26 July, values of K_z in the bottom layer were greater than during the low tidal range period, with values of $\sim 3 \times 10^{-3}$ m^2 s^{-1} to $\sim 2 \times 10^{-2}$ m^2 s^{-1}(and $\sim 3 \times 10^{-3}$ to $\sim 2 \times 10^{-2}$ m^2 s^{-1} within the water column based on the salt budget).

6. Discussion

6.1. Tidally Averaged Circulation and Salt Transport Characteristics

[48] Observed velocity profiles (Figure 5) and the tidally averaged velocities (Figure 10a) provide evidence that the CFRE estuary exhibits characteristics of a classic two-layer estuarine system in which density-driven circulation enhances inflow near the bottom and fresher and less dense water flows out near the surface. On the basis of circulation and stratification parameters defined in *Hansen and Rattray*'s [1966] classification scheme, the CFRE may be classified as a "Type 2b" estuary in which flow reverses at depth, appreciable stratification exists, and both advection and tidal diffusion are significant in determining the upstream salt flux during each sampling period. Analysis of horizontal salt fluxes suggests tidally driven salt transport is significant around middepth, near the tidally averaged location of the pycnocline, and that mean advective transport dominates near the bottom during both tidal range periods (Figures 10d and 10e). Analyses of salinity profiles at the

Table 1. Computed Tidally Driven Salt Fluxes Based on the Oscillatory Representations and Computed Tidally Driven Salt Fluxes Based on the Salt Flux Equation for 12 July and 26 July

Depth Below Surface (m)	Tidally Driven Salt Flux (Oscillatory Representation) (m s^{-1})	Tidally Driven Salt Flux (Salt Budget Equation) (m s^{-1})
	12 July	
2	0.31	0.31
3	0.56	0.54
4	0.72	0.69
5	0.91	0.89
6	0.86	0.84
7	0.61	0.58
8	0.26	0.29
9	0.09	0.10
10	−0.06	−0.04
11	−0.12	−0.08
12	−0.10	−0.07
	26 July	
2	0.66	0.58
3	0.65	0.64
4	0.87	0.90
5	0.98	1.07
6	0.83	1.00
7	0.64	0.69
8	0.42	0.41
9	0.24	0.26
10	0.09	0.07
11	0.01	−0.02
12	−0.05	−0.07

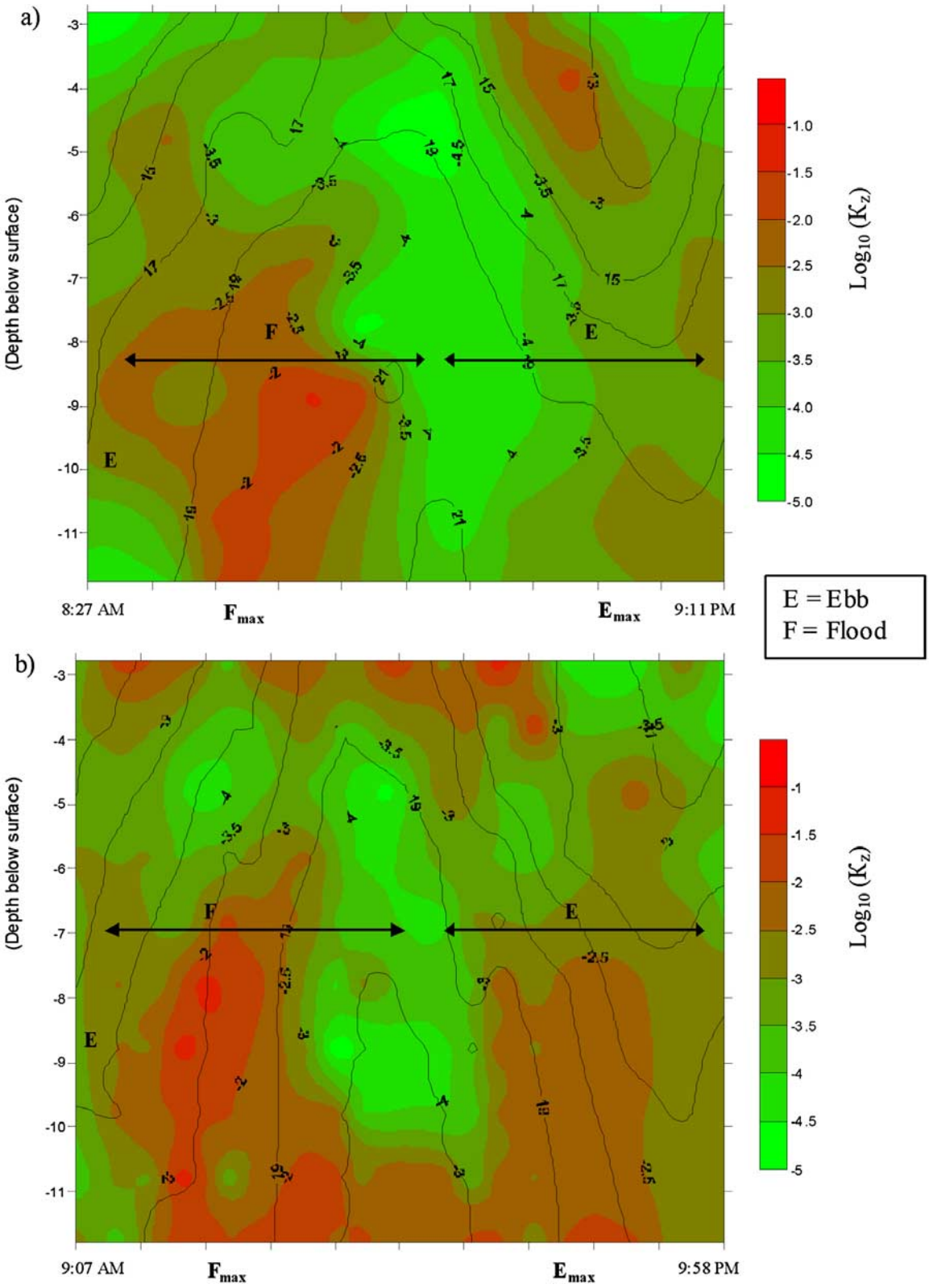

Figure 13. Log_{10} (K_z) using *Munk and Anderson*'s [1948] eddy diffusivity coefficient formulation ($C_d = 0.001$) and salinity contours at M44 on (a) 12 July and (b) 26 July. "F_{max}" and "E_{max}" represent times of maximum flood and ebb velocities, respectively.

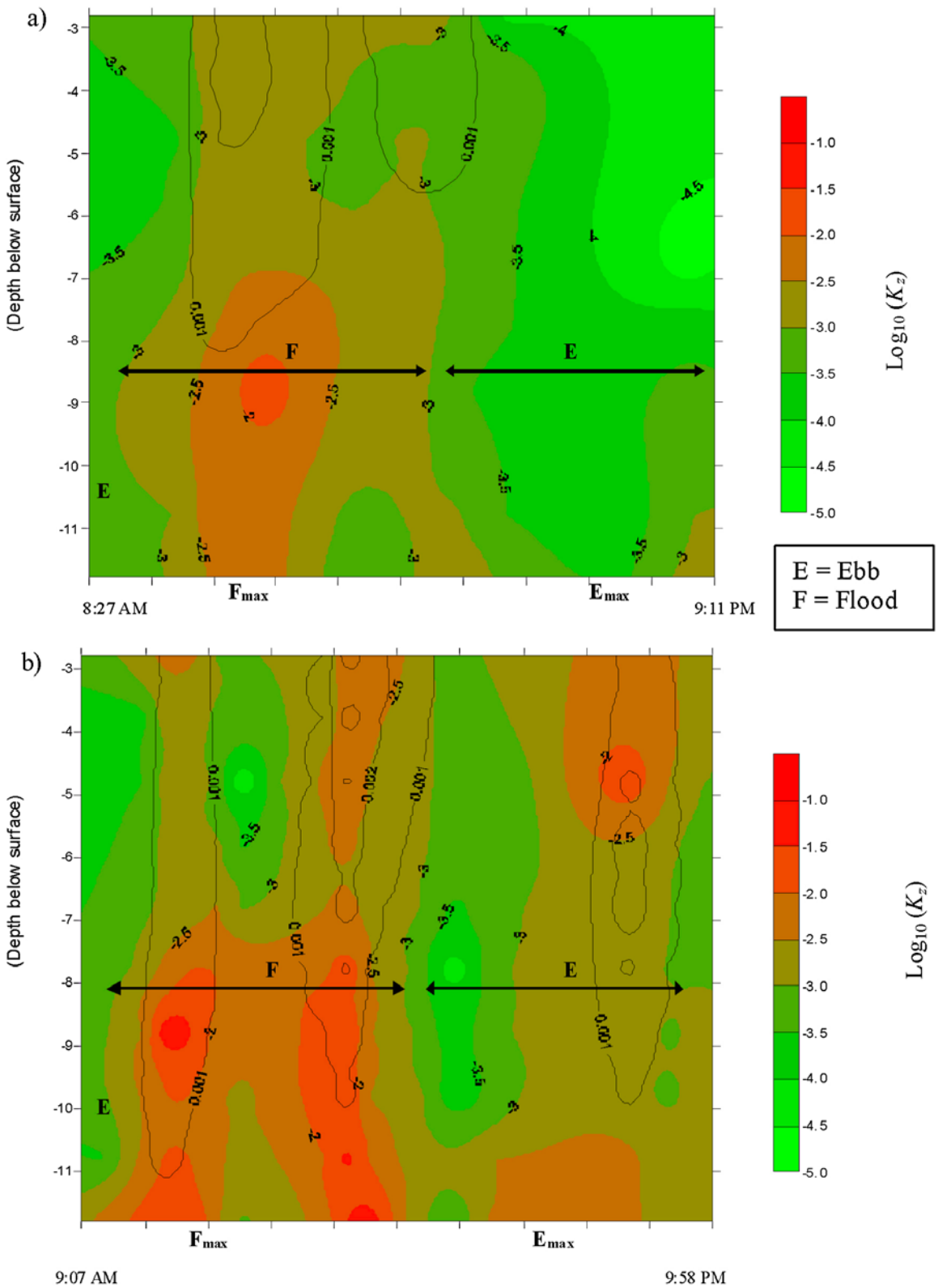

Figure 14. Log_{10} (K_z) together with contours of estimated vertical turbulent salt fluxes calculated from a simplified salt budget equation on (a) 12 July and (b) 26 July. "F_{max}" and "E_{max}" represent times of maximum flood and ebb velocities, respectively.

stations from the field study (e.g., Figure 9) are consistent with historical data showing a trend of increased near-bottom salinities during the low-tidal range period (Figure 2).

[49] Velocity data collected as part of the present study does not show increased net circulation during the low tidal range sampling period, as has been observed in other estuaries with significant gravitational circulation [*Blanton et al.*, 2003; *Bowen and Geyer*, 2003]. Rather, our results indicate that tidally averaged near-bottom along-channel velocities are greater during higher tidal range conditions than during lower tidal range conditions (Figure 10a). The pattern is consistent with results that would be expected on the basis of differences in the horizontal density gradients during the two periods. Stronger depth-averaged horizontal density gradients during the higher tidal range period (-0.6 km^{-1} on 26 July versus -0.5 km^{-1} on 12 July) would allow for increased baroclinic circulation. A sharp increase in the computed baroclinic acceleration in the lower portion of the water column on 26 July provides further evidence that the increased tidally averaged velocities in the lower part of the water column are a result of increased density-driven flow during the higher tidal range period (Figures 10a and 10c).

[50] Analysis of tidally and depth-averaged total salt fluxes indicates a net upstream (mean advective and tidal) flux of salt occurs in the main channel during both tidal range periods. Both mean advective and tidal fluxes were slightly greater during the higher tidal range period. During the low tidal range period, about 60% of the total salt flux was attributable to advection with the remaining flux resulting from tidal processes. During the higher tidal range period, mean advective salt transport accounted for approximately half of the total salt flux. We hypothesize these residual upstream salt fluxes in the main channel are balanced by a seaward salt flux over the shoals where shallower depths may prevent strong up-estuary baroclinic transport.

[51] Comparison of tidally driven horizontal salt fluxes based on the simple salt budget equation (equation (3)) to those computed from harmonic analysis of tidal salinity and velocity variations (equation (6)) indicates a close agreement exists (Table 1). The time-varying horizontal salt fluxes, based on equation (3), are largely attributable to oscillatory salt transport (variations in the tidal velocity and salinity fields). Increased oscillatory salt fluxes near middepth (Figures 10d and 10e; Table 1) occur as a result of relatively large amplitudes (compared to other parts of the water column) of tidal velocity and tidal salinity variations (U_o and S_o) and small phase differences ($\phi_u - \phi_s$). In the lower part of the water column, in contrast, reduced oscillatory salt fluxes occur as a result of diminished amplitudes (U_o and S_o) and phase differences closer to quadrature (Figure 12).

[52] During the higher tidal range period, slightly greater tidally driven salt fluxes occur ($\sim$1 m s^{-1} on 26 July versus 0.9 m s^{-1} on 12 July at $\sim$5 m below surface) as a result of greater amplitudes of tidal salinity and velocity variations (U_o and S_o). Increased phase differences (i.e., ($\phi_u - \phi_s$) closer to quadrature compared to during the lower tidal range period) prevent significantly stronger oscillatory salt transport from occurring.

[53] Tidally driven salt fluxes in the CFRE reach maximum values around middepth where tidally averaged stratification is greatest. A similar pattern, in which relatively large up-estuary, tidally driven salt transport at middepth has been observed (e.g., Columbia River Estuary), has been linked to an internal tide during highly stratified periods [*Jay and Smith*, 1990b]. Comparisons of tidally driven transport during low versus high tidal range periods in the CFRE indicate the pattern is similar to the behavior observed in the Hudson River Estuary, where oscillatory salt transport does not show a clear spring-neap signature because increases in amplitudes of tidal velocity and salinity are compensated by phase shifts toward quadrature [*Bowen and Geyer*, 2003]. We note that the vertical structure of the oscillatory salt transport in the CFRE, however, differs from that observed in the Hudson River Estuary where largest values were found to occur closer to the surface [*Bowen and Geyer*, 2003].

[54] Salinity characteristics during different tidal range periods in CFRE are similar to those observed in estuaries with significant estuarine gravitational circulation (e.g., Hudson River, Satilla) in which increased near-bottom salinities occur during the low tidal range periods [*Blanton et al.*, 2003; *Bowen and Geyer*, 2003]. The mechanisms leading to this pattern in the CFRE, however, are different from the behavior observed in those systems, as our data indicate net near-bottom flow and computed horizontal salt fluxes do not increase during the low tidal range period. Thus, increased salinities in the CFRE during the low tidal range period may not be explained by increased up-estuarine transport due to stronger gravitational circulation.

[55] Modeling studies by *Park and Kuo* [1996] and *Weisberg and Zheng* [2003] suggested that increased vertical exchange of momentum resulting from increased vertical mixing can *weaken* gravitational circulation (as found in previous observational studies) or that increased vertical mixing can increase the horizontal salinity gradient and consequently can *strengthen* gravitational circulation (as observed in the CFRE). Changes in estuarine circulation with increased mixing were predicted from the dimensionless ratio (δ):

$$\delta = \frac{\left(\frac{\partial s}{\partial x}\right)_H}{\left(\frac{\partial s}{\partial x}\right)_L}\left[\frac{(U_t)_H}{(U_t)_L}\right]^{-1} \tag{11}$$

where U_t is tidal current amplitude and subscripts H and L represent variables during conditions of higher and lower mixing (e.g., higher tidal range period and lower tidal range period), respectively. As mixing increases, the dimensionless ratio predicts that estuarine circulation increases if $\delta > 1$ and decreases if $\delta < 1$ [*Park and Kuo*, 1996].

[56] On the basis of the observational data in the CFRE, the fractional change in the depth-averaged and tidally averaged horizontal salinity gradient was 1.2, while the fractional change in tidal amplitude was 1.3. The value of the dimensionless ratio (δ = 0.9) was not consistent with observations of increased estuarine circulation during the higher tidal range period. Given the simplifying assumptions and approximate nature of this balance, however, the value may be close enough to unity that the analysis is not able to discriminate the behavior from the observations.

[57] We note that data limitations (e.g., a lack of reliable vertical-velocity measurements) prevented accurate assessment of ratios based on energy considerations [*Weisberg and Zheng*, 2003]. To further understand the behavior of

the CFRE, we discuss differences in vertical mixing characteristics and their influence on salt transport in the following section.

6.2. Vertical Turbulent Mixing Characteristics

[58] Mixing characteristics during the two tidal range periods were compared by examining vertical turbulent salt fluxes and K_z values (Figure 14). During the low tidal range flood, relatively large values of turbulent vertical salt fluxes ($\sim 1 \times 10^{-3}$ to 2×10^{-3} m s^{-1}) occur when the pycnocline is close to the surface and along-channel velocities are relatively high (e.g., near maximum flood). Areas of relatively high vertical turbulent salt flux are generally constrained to the upper parts of the water column. During the higher tidal range flood, in contrast, greater values of vertical turbulent salt fluxes ($\sim 1 \times 10^{-3}$ to 3×10^{-3} m s^{-1}) extend throughout much of the water column. During the high tidal range period, relatively large values also occur during the ebb tide in the vicinity of the pycnocline (Figure 8).

[59] Examination of estimated K_z values calculated from the salt budget equation (Figure 14) indicates that on 12 July, K_z values were relatively low ($\sim 2 \times 10^{-4}$ to $\sim 2 \times 10^{-3}$ m^2 s^{-1}) except near maximum flood tide below the pycnocline (when K_z values reach $\sim 2 \times 10^{-2}$ m^2 s^{-1} in the lower portion of the water column). These higher values of K_z in the lower part of the water column (as opposed to higher values of turbulent salt flux in the upper water column) result from more well mixed conditions closer to the bed (i.e., bottom generated shear and associated turbulence would be expected to contribute to well mixed conditions in the lower water column). On 26 July, relatively high values of K_z are found during much of the flood tide (e.g., $\sim 1 \times 10^{-2}$ m^2 s^{-1} to $\sim 9 \times 10^{-2}$ m^2 s^{-1} near the bottom part of the water column), and increased values of K_z (relative to the lower tidal range period) extend into the upper water column (e.g., $\sim 3 \times 10^{-3}$ up to $\sim 8 \times 10^{-3}$ m^2 s^{-1}). The analysis is consistent with observations (Figure 8) that relatively salty water may reach upper parts of the water column during the higher tidal range flood tide (as a result of increases in turbulent mixing) but that relatively salty water is constrained to the lower water column during the lower tidal ranges (as a result of weaker mixing). The observed differences are presumably a result of differences in the turbulence from bed-generated shear during the two tidal range periods.

[60] During the ebb tide, K_z values remain relatively low on 12 July ($\sim 1 \times 10^{-4}$ to $\sim 9 \times 10^{-4}$ m^2 s^{-1}). On 26 July, greater K_z values ($\sim 3 \times 10^{-3}$ to $\sim 2 \times 10^{-2}$ m^2 s^{-1}) relative to low tidal range observations following the ebb tide velocity maximum (Figure 14) provide evidence that mixing of fresh and salty water contribute to a reduction in near-bottom salinities observed during the high tidal range period. We note that these increased K_z values during the high tidal range ebb tide are consistent with patterns observed using the theoretical [*Munk and Anderson*, 1948] formulations of K_z (Figure 13).

[61] Negative values of K_z from the salt budget analysis occur near maximum ebb tide during both high and low tidal range periods and are presumably due to the significance of effects not included in our simplified salt balance, equation (10), such as cross-channel transport, vertical velocities, or internal waves.

[62] Our results indicate differences in vertical mixing characteristics (e.g., mixing of fresh and salty water during the higher tidal range conditions) contribute to differences in the observed near-bottom salinities. Increased turbulent vertical salt fluxes (>0.001 m s^{-1}) during the higher tidal range ebb tide occur around middepth (Figure 14b). The analysis provides evidence that the breach in stratification and reduced near-bottom salinities during the higher tidal range ebb tide (Figure 8b) are a result of a combination of midcolumn turbulence near the pycnocline (Figure 14b) and increased bed-generated mixing (Figures 13b and 14b).

[63] The effects of the increased vertical mixing during the higher tidal range period are evident in the tidally averaged salinity structure (Figure 10b). In the lower portion of the water column, salinities are greater during the lower tidal range period. Above $\sim$2 m below surface, salinities are greater during the higher tidal range period, as increases in turbulent mixing allow saltier water to reach the mid and upper parts of the water column.

[64] To summarize, our findings indicate that increased mixing during the higher tidal range period results in diminished stratification (as a result of increased midcolumn and bed-generated turbulence) and consequent freshening of near-bottom water. The freshening of near-bottom water leads to the stronger observed horizontal salinity gradient (shorter salinity intrusion length), and the resulting increase in baroclinic acceleration is strong enough (relative to frictional inhibition) to generate the observed increased gravitational circulation in the lower water column during the higher tidal range period (Figures 10a and 10c).

7. Conclusion

[65] Our analysis provides insights into mechanisms that influence along-channel circulation and salt transport patterns for varying tidal conditions in the CFRE when river inflow is low and relatively constant. Observations of the velocity and density structure indicate the CFRE exhibits characteristics of a classic (“Type 2b”) two-layer estuarine system [*Hansen and Rattray*, 1966] in which flow reverses at depth, appreciable stratification exists, and both gravitational estuarine circulation and tidal diffusion are significant in determining the upstream salt flux. Tidally driven salt fluxes resulting from oscillatory salt transport (variations in tidal velocities and salinities) are dominant around middepth (near the pycnocline) and mean advective transport dominates near the bottom during both low and higher tidal range periods. Approximately 50% to 60% (during higher and low tidal ranges, respectively) of the total horizontal salt fluxes were attributable to mean advective transport with the remaining flux resulting from tidal processes. We hypothesize upstream salt fluxes in the main channel are balanced by a seaward salt flux over the shoals.

[66] Findings indicate the horizontal and vertical salinity structure is significantly impacted by tidal range differences and intratidal (flood-ebb) variations. For the low tidal range period, near-surface to near-bottom stratification was relatively strong throughout the flood-ebb cycle, a well defined pycnocline persisted, and near-bottom salinities were relatively high. During the higher tidal range period the stratification varied with flood-ebb cycles and near-bottom salinities were relatively low. Residual flow, based on tidally

averaged near-bottom along-channel velocities, was greater during higher tidal range conditions than during lower tidal range conditions. This trend of increased residual flow during the higher tidal range period is different from patterns observed in other estuaries with significant gravitational circulation where decreased net flow has been observed during spring tides [*Nunes and Lennon*, 1987; *Linden and Simpson*, 1988; *Nunes et al.*, 1989; *Blanton et al.*, 2003]. Our analysis indicates the increase in tidally averaged circulation during the higher tidal range period in the CFRE is a result of a stronger horizontal salinity gradient and increased baroclinic acceleration in the lower portion of the water column.

[67] Previous research characterizing the behavior of estuarine circulation suggests residual circulation increases during periods of reduced turbulence such as during low tidal ranges [*Linden and Simpson*, 1988; *Stacey et al.*, 2001]. In estuaries with significant gravitational circulation, increased up-estuary salt transport during low tidal range periods has been found to coincide with periods of increased gravitational circulation [*Blanton et al.*, 2003; *Bowen and Geyer*, 2003]. Our analyses of data collected in this study together with historical data indicate that near bottom salinities in the CFRE increase during low tidal range periods (as has been observed in other estuaries) but that the increase may not be attributed to increases in estuarine gravitational salt transport. Rather, our analysis indicates that differences in vertical turbulent mixing characteristics, parameterized in this work through computed values of coefficients of vertical eddy diffusivity (K_z) and vertical turbulent salt fluxes, contribute to the differences in observed near-bottom salinities.

[68] A classic explanation for increased near-bottom salinities during low tidal ranges is that during periods of increased stratification (e.g., during neap tides), tidal mixing is inhibited, baroclinic circulation strengthens, and density-driven, up-estuary salt transport increases [*Monismith et al.*, 1996; *Li et al.*, 1998; *Stacey et al.*, 2001]. Our findings in the CFRE, in contrast, provide evidence that stronger tidal forcing and associated mixing contribute to (1) increased baroclinic circulation resulting from greater near-bottom horizontal salinity gradients and (2) greater transport of salt between the upper and lower portions of the water column and, as a result, lower near-bottom salinities. That is, during the higher tidal range period, vertical mixing increases, near-bottom horizontal salinity gradients are greater, and baroclinic circulation strengthens. As a result of increased mixing and weaker middepth stratification, however, fresher water is allowed to reach the bottom portion of the water column and contributes to lower observed near-bottom salinities.

[69] **Acknowledgments.** We thank John Bane, Larry Band, and Mike Mallin for their input on this work. We also thank Narayan Rajbhandari, Jim Bowen, Dianne Reid, Jim Fisher, Harold Quidley, Joe Purifoy, and Matthew McIver for assistance with the field study. Funding for this work was provided by an Environmental Protection Agency (EPA) STAR Grant (R-82867701-0) and by the University of North Carolina at Chapel Hill. Field data collection was conducted in collaboration with the North Carolina State Division of Water Quality.

References

Becker, M. L. (2007), Hydrodynamic behavior of the Cape Fear River estuarine system, North Carolina, Ph.D. dissertation, 111 pp., Univ. of N. C. at Chapel Hill, Chapel Hill.

Benson, H. A., and J. W. Parmen (1995), *Field Data Collection Report, Cape Fear River, Wilmington, North Carolina*, 193 pp., U.S. Army Corps of Eng. Waterw. Exp. Sta., Vicksburg, Miss.

Blanton, J. O., H. Seim, C. Alexander, J. Amft, and G. Kineke (2003), Transport of salt and suspended sediments in a curving channel of a coastal plain estuary: Satilla River, GA, *Estuarine Coastal Shelf Sci.*, *57*, 993–1006, doi:10.1016/S0272-7714(03)00005-2.

Bowen, M. M., and W. R. Geyer (2003), Salt transport and the time-dependent salt balance of a partially stratified estuary, *J. Geophys. Res.*, *108*(C5), 3158, doi:10.1029/2001JC001231.

Dyer, K. R. (1974), The salt balance in stratified estuaries, *Estuarine Coastal Mar. Sci.*, *2*, 273–281, doi:10.1016/0302-3524(74)90017-6.

Dyer, K. R. (1997), *Estuaries*, 2nd ed., 195 pp., John Wiley, New York.

Fischer, H. B. (1972), Mass transport mechanisms in partially stratified estuaries, *J. Fluid Mech.*, *53*(4), 671–687, doi:10.1017/S0022112072000412.

Hansen, D. V., and M. Rattray (1965), Gravitational circulation in straits and estuaries, *J. Mar. Res.*, *23*, 104–122.

Hansen, D. V., and M. Rattray (1966), New dimensions in estuary classification, *Limnol. Oceanogr.*, *11*, 319–326.

Jay, D. A. (1991), Internal asymmetry and anharmonicity in estuarine flows, in *Tidal Hydrodynamics*, edited by B. B. Parker, pp. 403–418, John Wiley, New York.

Jay, D. A., and J. D. Smith (1990a), Residual circulation in shallow estuaries: 2. Weakly stratified and partially mixed estuaries, *J. Geophys. Res.*, *95*, 733–748, doi:10.1029/JC095iC01p00733.

Jay, D. A., and J. D. Smith (1990b), Circulation, density distribution, and neap-spring transitions in the Columbia River Estuary, *Prog. Oceanogr.*, *25*, 81–112, doi:10.1016/0079-6611(90)90004-L.

Kjerfve, B. (1986), Circulation and salt flux in a well mixed estuary, in *Physics of Shallow Estuaries and Bays*, *Coastal Estuarine Stud.*, vol. 16, edited by J. van de Kreeke, pp. 22–29, Springer-Verlag, New York.

Li, C., A. Valle-Levinson, K. C. Wong, and K. Lwiza (1998), Separating baroclinic flow from tidally induced flow in estuaries, *J. Geophys. Res.*, *103*, 10,405–10,417, doi:10.1029/98JC00582.

Linden, P. F., and J. E. Simpson (1988), Modulated mixing and frontogenesis in shallow seas and estuaries, *Cont. Shelf Res.*, *8*(10), 1107–1127, doi:10.1016/0278-4343(88)90015-5.

McAdory, R. T., Jr. (2000), *Cape Fear-Northeast Cape Fear River, North Carolina Numerical Model Study*, 95 pp., U.S. Army Corps of Eng. Eng. Res. Dev. Cent. Coastal and Hydraul. Lab., Vicksburg, Miss.

Monismith, S., J. R. Burau, and M. Stacey (1996), Stratification dynamics and gravitational circulation in northern San Francisco Bay, in *San Francisco Bay: The Ecosystem*, edited by J. T. Hollibaugh, pp. 123–153, Am. Assoc. for the Adv. of Sci., San Francisco, Calif.

Munk, W. H., and E. R. Anderson (1948), Notes on a theory of the thermocline, *J. Mar. Res.*, *3*, 276–295.

Nepf, H. M., and W. R. Geyer (1996), Intratidal variations in stratification and mixing in the Hudson estuary, *J. Geophys. Res.*, *101*(C5), 12,079–12,086, doi:10.1029/96JC00630.

Nunes, R. A., and G. W. Lennon (1987), Episodic stratification and gravity currents in a marine environment of modulated turbulence, *J. Geophys. Res.*, *92*, 5465–5548, doi:10.1029/JC092iC05p05465.

Nunes, R. A., G. W. Lennon, and J. R. de Silva Samarasinghe (1989), The negative role of turbulence in estuarine mass transport, *Estuarine Coastal Shelf Sci.*, *28*, 361–377, doi:10.1016/0272-7714(89)90085-1.

Officer, C. B. (1976), *Physical Oceanography of Estuaries*, 465 pp., John Wiley, New York.

Park, K., and A. Y. Kuo (1996), Effects of variation in vertical mixing on residual circulation in narrow, weakly nonlinear estuaries, in *Buoyancy Effects on Coastal and Estuarine Dynamics*, *Coastal Estuarine Stud.*, vol. 48, edited by D. G. Aubrey and C. T. Friedrichs, pp. 301–317, AGU, Washington, D. C.

Prandle, D. (1985), On salinity regimes and vertical structure of residual flows in narrow tidal estuaries, *Estuarine Coastal Shelf Sci.*, *20*, 615–635, doi:10.1016/0272-7714(85)90111-8.

Rippeth, T. P., N. R. Fisher, and J. H. Simpson (2001), The cycle of turbulent dissipation in the presence of tidal straining, *J. Phys. Oceanogr.*, *31*, 2458–2471, doi:10.1175/1520-0485(2001)031<2458:TCOTDI>2.0.CO;2.

Simpson, J. H., J. Brown, J. Matthews, and G. Allen (1990), Tidal straining, density currents, and stirring in control of estuarine stratification, *Estuaries*, *13*(2), 125–132, doi:10.2307/1351581.

Simpson, J. H., R. Vennell, and A. J. Souza (2001), The salt fluxes in a tidally energetic estuary, *Estuarine Coastal Shelf Sci.*, *52*, 131–142, doi:10.1006/ecss.2000.0733.

Stacey, M. T., and D. K. Ralston (2005), The scaling and structure of the estuarine boundary layer, *J. Phys. Oceanogr.*, *35*, 55–71, doi:10.1175/JPO-2672.1.

Stacey, M. T., J. R. Burau, and S. G. Monismith (2001), Creation of residual flows in a partially stratified estuary, *J. Geophys. Res.*, *106*(C8), 17,013–17,037, doi:10.1029/2000JC000576.

Weisberg, R. H., and L. Zheng (2003), How estuaries work: A Charlotte Harbor example, *J. Mar. Res.*, *61*, 635–657, doi:10.1357/002224003771815981.

Welch, J. M., and B. B. Parker (1979), Circulation and hydrodynamics of the lower Cape Fear River, North Carolina, *NOAA Tech. Rep. NOS 80*, 108 pp., Off. of Oceanogr. Circulatory Surv. Branch, Rockville, Md.

Wong, K.-C. (1994), On the nature of transverse variability in a coastal plain estuary, *J. Geophys. Res.*, *99*(C7), 14,209–14,222, doi:10.1029/94JC00861.

M. L. Becker and H. Seim, Department of Marine Sciences, University of North Carolina at Chapel Hill, CB 3300, Chapel Hill, NC 27599, USA. (beckerm@email.unc.edu)

R. A. Luettich Jr., Institute of Marine Sciences, 3431 Arendell Street, Morehead City, NC 28557, USA.